



Cent. Eur. J. Energ. Mater. 2023, 20(4): 369-385; DOI 10.22211/cejem/176594

Article is available in PDF-format, in colour, at:

<https://ipo.lukasiewicz.gov.pl/wydawnictwa/cejem-woluminy/vol-20-nr-4/>



Article is available under the Creative Commons Attribution-Noncommercial-NoDerivs 3.0 license CC BY-NC-ND 3.0.

Research paper

The Influence of Three Binders on the Properties of BTF-Based Composite Explosive

Wei Ji^{*}), Yuxuan Xu, Lei Liu, Changping Guo,
Xianfeng Wei, Dunju Wang

*School of Defense Science and Technology,
Southwest University of Science and Technology, Sichuan
Collaborative Innovation Center for New Energetic Materials,
Mianyang, Sichuan, 621010, China*

** E-mail: jiwei7327@163.com*

Abstract: Benzotrioxofurazan (BTF) -based composite explosives containing three different binder components were prepared in this study, using nitrocellulose (NC), thermoplastic polyurethane (Estane), and fluororubber 2602 (F₂₆₀₂) as binders, through the electrostatic spray method. The objective was to reduce the sensitivity of BTF. The BTF-based composite explosives were characterised using a range of scientific equipment, including scanning electron microscopy (SEM), Fourier Transform infrared spectroscopy (FT-IR), DSC thermal analysis, and mechanical sensitivity. The SEM results indicated that the BTF-based composite explosives' particle size was between 50 and 100 nm, and had a spherical shape. Compared with the raw BTF, the critical temperature of thermal explosion of the three composite explosives, BTF/NC, BTF/Estane and BTF/F₂₆₀₂, was increased by 4.21, 6.8 and 9.44 °C, respectively. These increases indicate an improvement in the thermal stability of the samples. The characteristic drop height of BTF/NC, BTF/Estane and BTF/F₂₆₀₂ was 68.12, 62.34 and >80 cm, respectively. Additionally, the explosion percentage of BTF/NC, BTF/Estane and BTF/F₂₆₀₂ had been decreased to 24%, 24%, and 8%, respectively. These results suggest a significant enhancement in the safety performance of all three samples.

Keywords: BTF-based composite explosive, electrostatic spray method, thermal stability, mechanical sensitivity

1 Introduction

As a zero oxygen non-hydrogen explosive, benzotrifuroxan (BTF, $C_6N_6O_6$, see Figure 1) has better initiation performance [1], output energy, mechanical sensitivity, and thermal stability than pentaerythritol tetranitrate (PETN, $C_5H_8N_4O_{12}$). Additionally, the detonation energy of BTF is equivalent to that of HMX, and the shock initiation sensitivity and misfire diameter are equivalent to those of 1,3,5,7-tetranitro-1,3,5,7-tetrazocane (HMX, $C_4H_8N_8O_8$). The BTF explosive has been effectively used in detonation cord charges and in the enhancement of the charge characteristics of composition B [2-4]. However, the BTF explosive exhibits sensitivity to mechanical impact, which makes it difficult to meet the requirements for good safety performance in modern weapon systems.

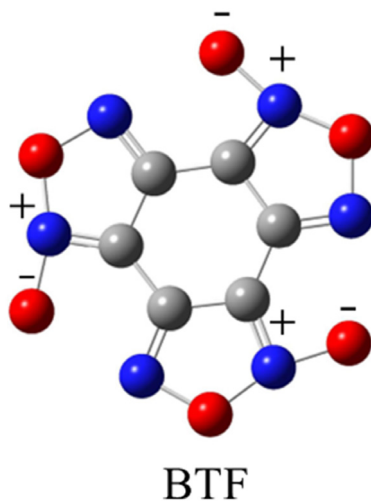


Figure 1. Structure of BTF

Consequently, numerous attempts have been undertaken to decrease its sensitivity and to achieve all the required aspects [5, 6]. These efforts mainly include modification of the crystal structure, refining crystal defects through recrystallization, and fabricating energetic composite materials by incorporating additives such as fluororubber and graphite. The production of energetic materials has demonstrated encouraging outcomes among other strategies. Hitherto, researchers from domestic and foreign organisations have proposed an array of successful techniques for manufacturing composite materials. This includes approaches such as the solvent-nonsolvent recrystallization method,

the microemulsion method, the aqueous suspension, the spray-drying method and the electrostatic spraying method.

Wang *et al.* [7] manufactured Al/Bi₂O₃-HNIW composite explosives using the solvent-nonsolvent technique, which demonstrated outstanding levels of safety and detonation performance, raising the possibility of using it as a replacement for the primary explosive in a detonator. Zhu *et al.* [8] fabricated CL-20/PNCB composite explosives with lowered impact sensitivity utilizing the microemulsion method. The characteristic drop height (5 kg drop weight) for raw CL-20 and CL-20/PNCB was 13 and 63 cm, respectively. Wang *et al.* [9] prepared CL-20/thermoplastic polyurethane elastomer rubber (Estane), *i.e.* CL-20/Estane, composite explosive using the water suspension technique. The characteristic height of CL-20/Estane composite particles increased from 34.8 to 39.8 cm on adding calcium stearate, and the thermal stability was improved to a certain extent. Wei *et al.* [10] prepared a HMX/copolymer of vinylidene fluoride and hexafluoropropylene (F₂₆₀₂), *i.e.* HMX/F₂₆₀₂, core-shell composite explosive using the spray-drying method. Compared to HMX/F₂₆₀₂ composite microspheres produced by the physical composite method, the impact characteristic drop height of HMX/F₂₆₀₂ core-shell composite microspheres was increased from 31.23 to 41.37 cm, respectively. Additionally, there was a significant decrease in the impact sensitivity.

In recent years, electrostatic spraying technology [11] has been regarded as having an enormous potential approach for producing composite explosives, due to its ability to rapidly prototype and easily control the sample's morphology and dimensions, as well as its low laboratory equipment requirements. With regard to explosives formulation, the binder plays a crucial role in the system. Although the binder makes up only a small proportion of the system, it has a significant impact on the safety performance of the explosive [12-14]. The addition of a binder has the potential to enhance the composition effect between various components, as well as to improve the mechanical properties and rheological properties of the charge, which in turn facilitates forming and processing [15, 16]. Simultaneously, the use of binders can significantly decrease the sensitivity of composite explosives. Therefore, a study of the effects of binders on the performance of BTF explosives is of great application value and practical importance. Based on these, BTF-based composite explosives were prepared by electrospray technology using BTF explosive as the main explosive, acetone as the solvent, and nitrocellulose (NC), Estane, and F₂₆₀₂ as the binding agents, respectively. The samples were then evaluated in terms of their morphology, structure, thermal decomposition and impact sensitivity. The prepared BTF-based composite explosives displayed considerable insensitivity

towards impact and thermal effects. This work potentially provides an alternative method for reducing the vulnerability and enhancing the transportation safety of BTF explosive. Therefore, BTF-based explosives present promising potential for their application in detonator charges.

2 Materials

BTF was prepared in the lab with a purity of 98%. Acetone was purchased from Chengdu Cologne Chemical Co., Ltd. Estane was supplied by Lubrizol Corporation; NC was provided by Luzhou North Chemical Industry Co., Ltd. F₂₆₀₂ was purchased from Huizhou Haoyuan Plastic Co., Ltd.

3 Preparation of BTF-based Composite Explosives

BTF-based composite explosives were prepared by electrostatic spraying technology. The experimental process is as shown in Figure 2. Firstly, raw BTF (0.5 g) was dissolved in acetone (5 mL) to give a solution with a concentration of 0.1 g·mL⁻¹. Secondly, the binder (Estane, NC or F₂₆₀₂) was dissolved in this solution. The mass ratio of binder to raw BTF explosive was 2:98. The transparent precursor solution was acquired by leaving the solution to settle and filtering it. Subsequently, the transparent precursor solution was transferred into a syringe and fed through a syringe pump at a rate of 0.05 mL·min⁻¹. The negative pressure recorded was -10.00 kV, and the positive pressure was +10.17 kV, as process conditions.

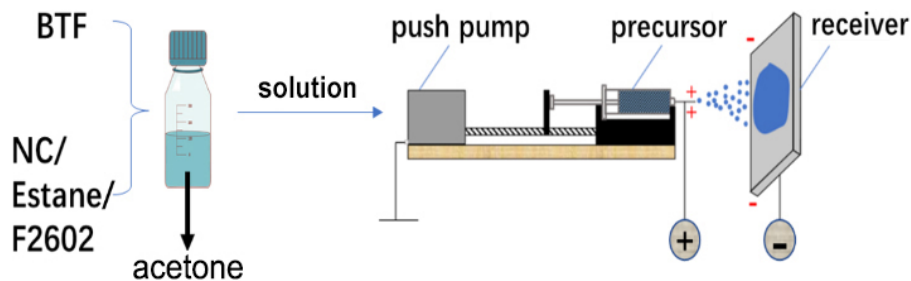


Figure 2. Schematic illustration of the preparation of BTF-based composite explosives by electrostatic spray

4 Test Methods

The morphology of the samples was analyzed with a Hitachi SU-8020 scanning electron microscope (SEM, Hitachi, Japan); the accelerating voltage was 10.0 kV. A Fourier transform infrared spectrometer (FT-IR, Bruck Optical Instruments Ltd) was used to further characterize the composition of the samples. The thermal decomposition properties of all samples were tested by thermogravimetry-differential scanning calorimetry (TG-DSC, Netsch GMBH, Germany); all samples were placed in Al₂O₃ crucibles, weight 0.7 ± 0.1 mg, and heated at 5, 10, and 20 K · min⁻¹ from 30 to 500 °C in a high-purity nitrogen purge with a flow rate of 60 mL · min⁻¹. The impact sensitivity and friction sensitivity of the samples were tested by W1-1 type drop hammer (Xi'an Modern Chemical Research Institute).

5 Results and Discussion

5.1 Morphological analysis

Typical SEM images of both raw BTF and the samples prepared by electrostatic spraying are shown in Figure 3. Figure 3(a) shows the SEM image of raw BTF, and exhibits an “ice cream” like structure with a rough and angular surface and a particle size between 5 and 10 μm. Figure 3(b) is the BTF/NC composite explosive, revealing that the surface of these spherical particles has become smoother, with an average particle size of about 500-900 nm. Figure 3(c) is the BTF/Estane composite explosive. The particles are either spherical or have a three-dimensional block structure, with a smooth surface and a narrow particle size distribution of approximately 50 nm. Figure 3(d) is the BTF/F₂₆₀₂ composite explosive, where the particles possess a spherical shape and densely coated particles are formed on their surface. The particle size is predominantly concentrated around 50 nm. Furthermore, the variegated morphology of the BTF-based composite explosives suggested dissimilar bonding states, which resulted from the incongruity of the viscosity of the solvent during the dissolution of the binder.

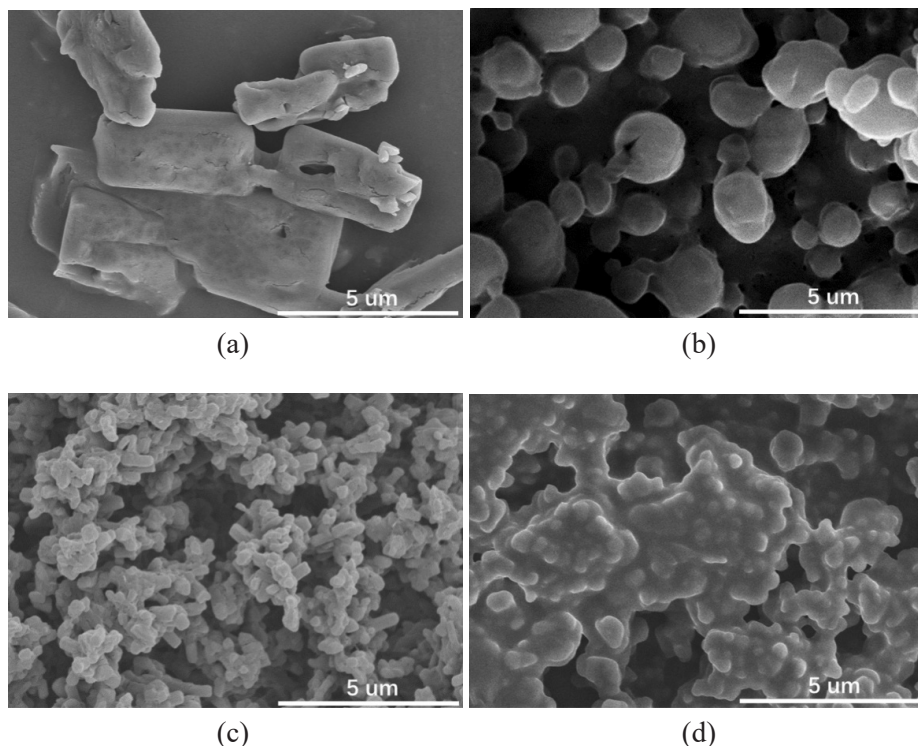


Figure 3 SEM images of the composite explosive samples: BTF (a), BTF/NC (b), BTF/Estane (c), and BTF/F₂₆₀₂ (d)

5.2 Structure and composition analysis

Elemental mapping, FT-IR was conducted to confirm the compositions. The infrared spectral curves of raw BTF, BTF/NC, BTF/Estane and BTF/F₂₆₀₂ are shown in Figure 4.

As can be seen from Figure 4, raw BTF exhibits the characteristic absorption bands of C=N at 1654 cm⁻¹, the deformation vibrations of -NO₂ at 1567 and 1418 cm⁻¹ and two other characteristic absorption peaks at 962 and 649 cm⁻¹, respectively. Estane exhibits a strong absorption peak at 1737 cm⁻¹, and F₂₆₀₂ exhibits a characteristic absorption peak at 1159 cm⁻¹. There are three strong peaks for NC at 1650, 1280 and 840 cm⁻¹ that are assigned to the inplane bending vibration of -ONO₂ groups (1650 and 1280 cm⁻¹) and the stretching vibration of C-O-NO₂ groups (840 cm⁻¹), respectively. By comparing the spectra of BTF/NC, BTF/Estane and BTF/F₂₆₀₂, it may be observed that the BTF/Estane composite explosive exhibits the same characteristic absorption peak at 1737 cm⁻¹ as raw Estane. The BTF/F₂₆₀₂ composite explosive showed a strong absorption peak at

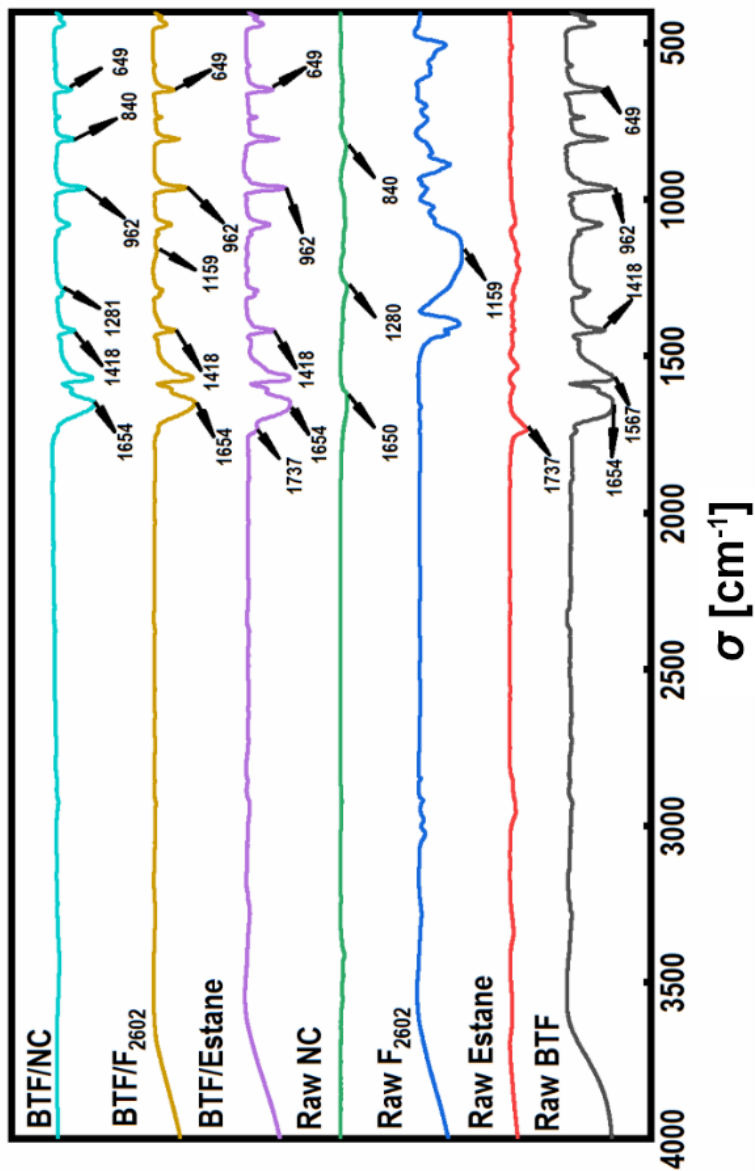
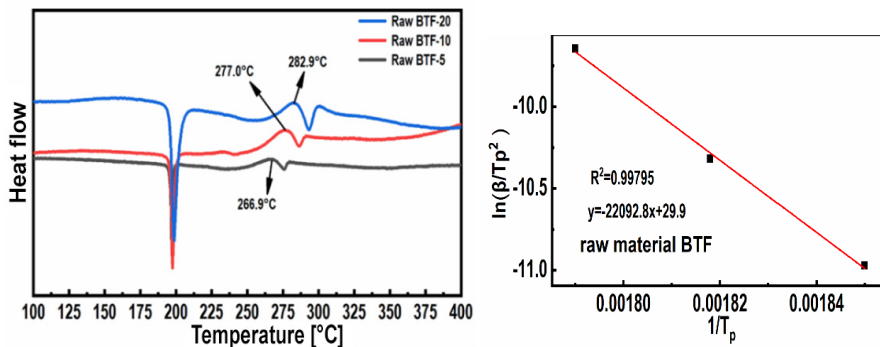


Figure 4. FT-IR spectra of the composite explosive samples and their precursors

1159 cm^{-1} , the same as raw F_{2602} . The absorption peaks of the BTF/NC composite explosive at 1654, 1418, 962 and 649 cm^{-1} correspond to those of raw BTF at 1650, 1418, 962 and 649 cm^{-1} . The absorption peaks of the BTF/NC composite explosive at 1281 and 840 cm^{-1} correspond to those raw NC at 1280 and 840 cm^{-1} . This shows that the three binders were successfully coated onto raw BTF during the electrostatic spray compounding process. Furthermore, no new diffraction peaks (or functional groups) were observed following compounding BTF with Estane, F_{2602} and NC, respectively. These observations indicate the absence of any chemical reactions between the three binders and BTF explosive, and that no new matter was produced as a result of the mixture.

5.3 Thermal decomposition

A simultaneous thermal analyzer was used to examine the thermal decomposition characteristics of raw BTF and the composite explosive samples at heating rates of 5, 10 and 20 $^{\circ}\text{C}\cdot\text{min}^{-1}$ in the temperature range of 100–400 $^{\circ}\text{C}$, as shown in Figure 5. When the heating rate was 10 $^{\circ}\text{C}\cdot\text{min}^{-1}$, two temperature peaks (an endothermic peak at 180–200 $^{\circ}\text{C}$ and an exothermic peak at 260–280 $^{\circ}\text{C}$) were evident in raw BTF and the composite explosive samples. The samples absorbed heat and melted between the temperature of 180–200 $^{\circ}\text{C}$, transforming from solid to liquid. They underwent complete decomposition as the temperature climbed to 260–280 $^{\circ}\text{C}$. Furthermore, an analysis of the DSC curves at heating rates of 5, 10 and 20 $^{\circ}\text{C}\cdot\text{min}^{-1}$, revealed an increase in the peak temperature of thermal decomposition (T_p) with increasing heating rate, accompanied by a broadening of the peak. On the other hand, there was hardly any change in the temperature of the melting peak. This suggests that the exothermic peak's shift to high temperature may be attributed to the increase in thermal effect per unit time and temperature difference.



(a)

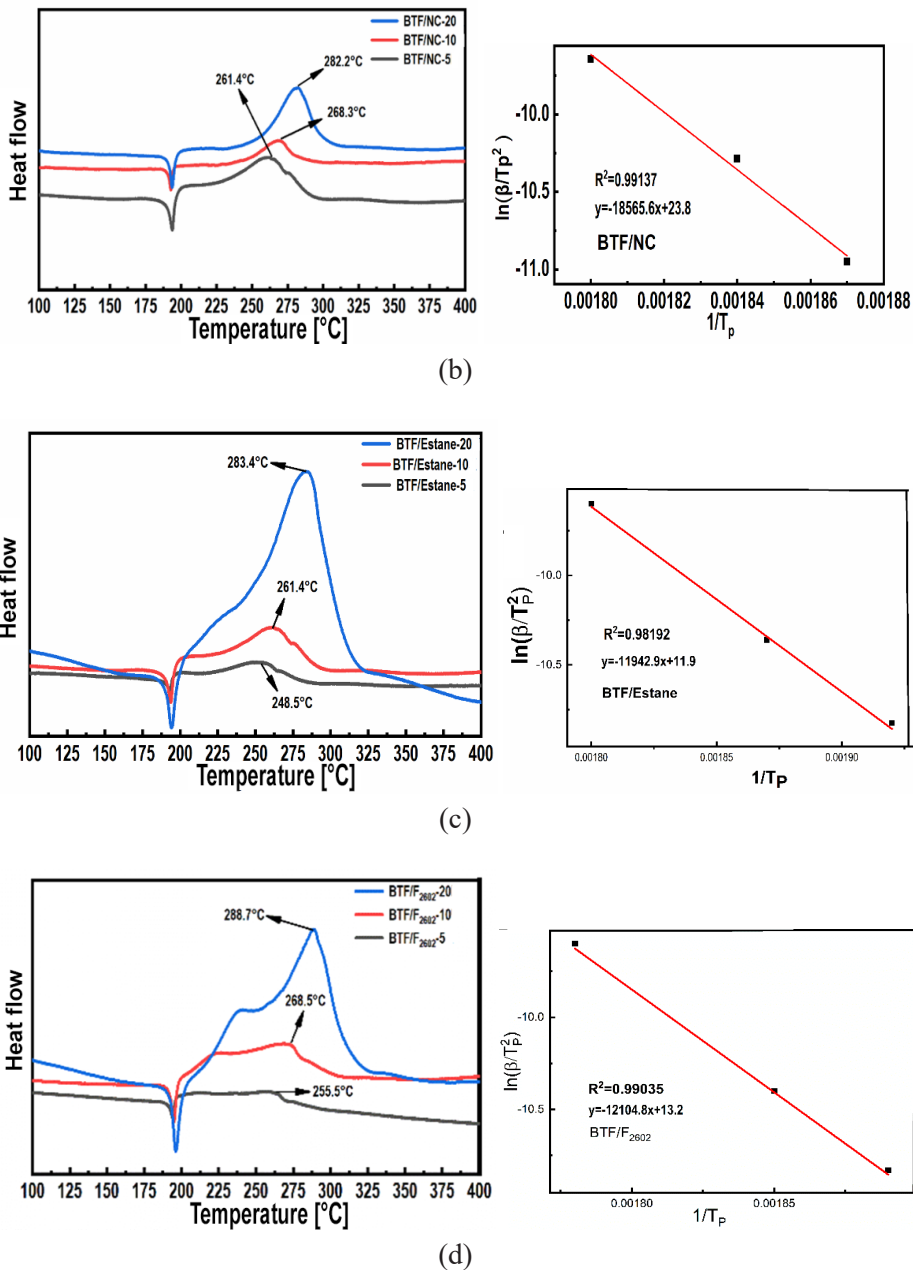


Figure 5. DSC curves and Kissinger plots for raw BTF (a), BTF/NC (b), BTF/Estane (c) and BTF/F₂₆₀₂ (d)

The thermal decomposition kinetics of raw BTF and of the composite explosive samples were calculated by the Kissinger formula (Equation 1), where E_a is the apparent activation energy, β is the heating rate, R is the gas constant and T_p is the peak temperature (Equation 2) and A is the frequency factor (Equation 3).

$$\ln\left(\frac{\beta_i}{T_{pi}^2}\right) = \ln\left(\frac{AR}{E_a}\right) - \frac{E_a}{RT_{pi}} \quad (1)$$

$$T_{pi} = T_{p0} + b\beta_i + c\beta_i^2 \quad (2)$$

$$A = \frac{kT_p}{h} \exp\left(\frac{\Delta S}{R}\right) \quad (3)$$

According to the Kissinger equation, the value of $\ln(\beta/T_p^2)$ was plotted against $1/T_p$ (see Figure 5). Based on the slope and intercept, the E_a and the A data for the thermal decomposition are shown in Table 1.

Table 1. Thermal decomposition kinetic parameters and thermal safety parameters of the samples

Sample	E_a [kJ·mol ⁻¹]	A [s ⁻¹]	T_{po} [°C]	T_b [°C]
BTF	183.40	$2.1 \cdot 10^{17}$	251.90	265.03
BTF/NC	154.34	$4.0 \cdot 10^{14}$	253.20	269.24
BTF/Estane	99.3	$1.7 \cdot 10^9$	254.00	271.83
BTF/F ₂₆₀₂	100.6	$6.5 \cdot 10^9$	256.60	274.47

It can be clearly seen in Table 1 that E_a values of BTF/NC, BTF/Estane and BTF/F₂₆₀₂, when compared with that of raw BTF, had decreased by 29.06, 84.1 and 82.8 kJ·mol⁻¹, respectively. This is because the activation energy level is related to the heat transfer rate of particles: the higher the heating rate is, the more the activation energy decreases. However, when the particle size of a BTF composite sample reached the nanometer level, the specific surface area had increased, resulting in an increase in the heat transfer rate and a decrease in the activation energy. It can be seen that the activation energy of the BTF/Estane sample had decreased the most, indicating that the heat transfer rate of the BTF/Estane sample is faster than that for the BTF/NC and BTF/F₂₆₀₂ samples. The critical temperature for thermal explosion (T_b) is a vital parameter in evaluating the safety of the materials and in ascertaining the transformation from thermal decomposition to thermal explosion.

Concurrently, the self-accelerating decomposition temperature (SADT) represents the maximum allowable ambient temperature for practical application. In order to calculate SADT, a polynomial regression method (Equation 2) was used. For $b = 0$, the initial decomposition temperature T_{p0} was obtained with greater precision, leading to $\text{SADT} = T_{p0}$. The critical temperature of thermal explosion (T_b) was obtained by substituting T_{p0} in Equation 4.

$$T_b = \frac{E_a - \sqrt{E_a^2 - 4RE_aT_{p0}}}{2R} \quad (4)$$

Compared to raw material BTF ($\text{SADT} = 251.90\text{ }^\circ\text{C}$, $T_b = 265.03\text{ }^\circ\text{C}$), the thermal explosion critical temperature and self-accelerated decomposition temperature of BTF/NC had increased by 1.3 and 4.21 $^\circ\text{C}$, respectively. The corresponding data for BTF/Estane exhibited an increase of 2.1 and 6.8 $^\circ\text{C}$, respectively, while for BTF/F₂₆₀₂ the figures were 4.7 and 9.44 $^\circ\text{C}$, respectively. These results indicate that the electrostatic spraying process improved the thermal safety and stability of the samples, with BTF/F₂₆₀₂ displaying the most significant enhancement.

The TG-DTG curves in Figure 6 illustrate the thermal decomposition of raw BTF and its composite explosives BTF/Estane, BTF/F₂₆₀₂ and BTF/NC at a heating rate of 10 $^\circ\text{C}\cdot\text{min}^{-1}$. As shown, raw BTF undergoes mass loss beginning at 186.3 $^\circ\text{C}$, with a 97.33% mass loss total. The composite explosives, BTF/Estane, BTF/F₂₆₀₂ and BTF/NC, exhibited lower mass losses of 89.04%, 91.49% and 89.41%, respectively. Compared to raw BTF, all three samples displayed varying degrees of mass loss reduction. This is due to the fact that the binder itself did not decompose during thermal decomposition, and a small part of the BTF did not decompose due to the uniform coating of the binder on the surface of the BTF particles, which indicates that the three binders were all well bonded to the raw BTF.

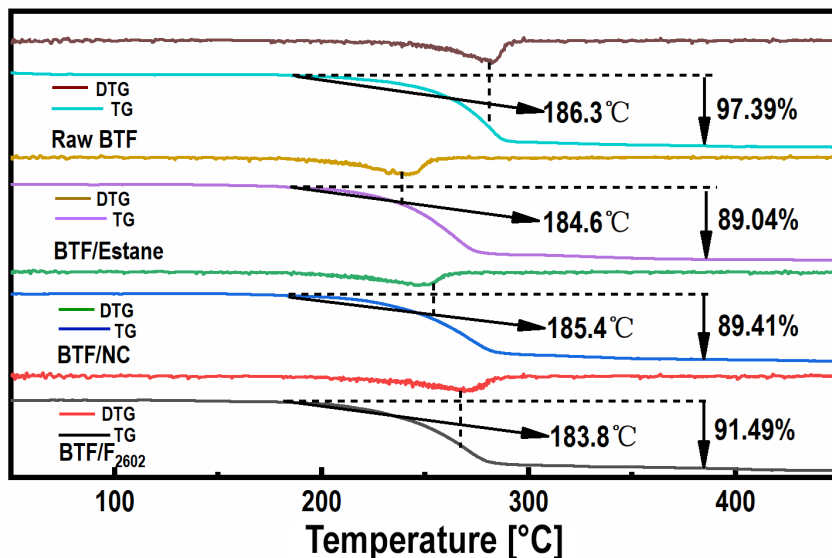


Figure 6. TG-DTG curves of the various samples

The thermal decomposition of explosives involves the activation and breaking of molecular bonds. As heat is applied to the explosive molecules, their molecular thermal movement is gradually enhanced, causing the molecular bonds to stretch. When the bonds are stretched to a certain extent, the weakest molecular bond break, resulting in energy changes. This process can be described by the enthalpy of activation (ΔH), Gibbs free energy of activation (ΔG) and entropy of activation (ΔS). The calculation equations are shown in Equations 3, 5 and 6.

$$\Delta H = E_a - R \cdot T_p \quad (5)$$

$$\Delta G = \Delta H - \Delta S \cdot T_p \quad (6)$$

Using the computed data, the results of these calculations (ΔH , ΔG , ΔS) are listed in Table 2. The results show that for raw BTF and the three composite explosive samples, the activation free energy ΔG is positive, indicating that the transition from the normal state to the transition state requires energy absorption rather than proceeding spontaneously. This implies that they can remain stable in the normal state. As evidenced by the calculated ΔS , the ΔS of the three samples is notably lower than that of raw BTF, indicating that the encapsulated BTF is less susceptible to decompose into gas during thermal decomposition.

Table 2. Thermal decomposition kinetic parameters and thermal safety parameters of the samples

Sample	ΔH [kJ·mol ⁻¹]	ΔS [J·mol ⁻¹]	ΔG [kJ·mol ⁻¹]
BTF	179.03	81.99	135.98
BTF/NC	149.69	21.66	138.29
BTF/Estane	94.92	-80.31	137.10
BTF/F ₂₆₀₂	96.20	-69.12	132.82

5.4 Compatibility

Compatibility is closely related to the safety and reliability of explosives. The compatibility of BTF based composite explosives was evaluated by determining the maximum peak temperature difference ΔT_p from the DSC curves, according to the criteria in Table 3. This can be calculated by the fitting results of the thermal analysis data. The evaluated corresponding compatibility values are summarized in Table 4.

Table 3. Compatibility criteria for the exothermic peak ΔT_p

ΔT_p [°C]	$\Delta E_a/E_a$ [%]	Content
≤ 2.0	≤ 20	Good compatibility
≤ 2.0	> 20	Moderately compatibility
> 2.0	≤ 20	Moderately incompatible
> 2.0	> 20	Incompatible

Table 4. Compatibility results of the BTF based composite explosives by DSC

Sample	E_a [kJ·mol ⁻¹]	T_{po} [°C]	ΔT_p (compared with raw BTF) [°C]	$\Delta E_a/E_a$ (compared with raw BTF) [%]
BTF	183.40	251.90	0	0
BTF/NC	154.34	253.20	1.3	15.8
BTF/Estane	99.30	254.00	2.1	45.8
BTF/F ₂₆₀₂	100.60	256.60	4.7	45.1

As demonstrated in Table 4, the exothermic peak temperature (ΔT_p) varies by only 1.3 °C (less than 2.0 °C) between BTF and the mixture NC and BTF. Additionally, the $\Delta E_a/E_a$ value is 15.8%. According to the compatibility evaluation criteria outlined in Table 3 for explosives and contact materials, NC and BTF have good compatibility. By contrast, there is a significant difference in the exothermic peak temperature (ΔT_p) of BTF and BTF/Estane and BTF/F₂₆₀₂ (2.1 and 4.7 °C,

respectively), and the $\Delta E_a/E_a$ value of BTF/Estane and BTF/F₂₆₀₂ (45.8% and 45.1%, respectively). Therefore, Estane and F₂₆₀₂ are incompatible with BTF.

5.5 Mechanical sensitivity

Mechanical sensitivity is one of the key parameters for evaluating the safety performance of energetic materials. The most direct physical factors that explosives encounter are mechanical forces such as friction and impact. Hence, the mechanical sensitivity of the materials BTF, BTF/NC, BTF/Estane and BTF/F₂₆₀₂ were investigated. Impact sensitivity and friction sensitivity were tested and their results are listed in Table 5.

Table 5. Mechanical sensitivity of the tested samples

Sample	Impact sensitivity (H_{50}) [cm]	Friction sensitivity [%]
Raw BTF	23.00	72
BTF/NC	68.12	24
BTF/Estane	62.34	24
BTF/F ₂₆₀₂	>80	8

Table 5 demonstrates that the mechanical sensitivities of BTF/NC, BTF/Estane and BTF/F₂₆₀₂ are significantly lower than those of BTF. Notably, compared to raw BTF ($H_{50} = 23.00$ cm), the characteristic drop heights of BTF/NC, BTF/Estane and BTF/F₂₆₀₂ were 68.12, 62.34 and over 80 cm, respectively. The friction sensitivity values of BTF/NC, BTF/Estane and BTF/F₂₆₀₂ were 24%, 24% and 8%, respectively, indicating a significant improvement in safety. Furthermore, BTF/F₂₆₀₂ had lower impact and friction sensitivities than BTF/NC and BTF/Estane, attributed to the formation of a cladding layer on the surface of the BTF particles by F₂₆₀₂ (refer to Figure 3). Factors affecting the mechanical sensitivity are as follows:

- (i) The electrostatic spray drying process reduces the particle size of BTF/NC, BTF/Estane and BTF/F₂₆₀₂, all reaching the nanoscale, and the reduction in crystal size minimizes crystal defects, all of which help to avoid the formation of “hot spots”.
- (ii) After compounding the binders NC, Estane and F₂₆₀₂ respectively with BTF, the binder acts as a “shock absorber”, consequently reducing the friction and external impact between the explosive particles, thus lowering the likelihood of “hot spot” formation.

6 Conclusions

- ◆ The BTF/NC, BTF/Estane and BTF/F₂₆₀₂ samples, prepared by the electrostatic spray method, exhibited a regular shape and had a particle size ranging from 500 to 900 nm. The infrared analysis indicated that there was no chemical reaction between NC, Estane, F₂₆₀₂ and the BTF explosive, and were physical mixtures.
- ◆ Although the production of BTF-based explosives using electrostatic spraying technology has numerous advantages in producing energetic materials, its yield is inadequate. Expanding production scale is the primary evaluation index in industrial production, and reduced yield significantly increases costs, so increasing the yield is a critical issue that needs to be resolved.
- ◆ Compared with raw BTF, the critical temperature of thermal explosion of BTF/NC, BTF/Estane and BTF/F₂₆₀₂ explosives had increased by 4.21, 6.80 and 9.44 °C, respectively. The above data imply that the addition of binder can effectively enhance the thermal stability of BTF, with NC exhibiting the most significant effects.
- ◆ Moreover, NC exhibits good compatibility with raw BTF, while Estane and F₂₆₀₂ are not compatible.
- ◆ The introduction of a binder also results in reduced impact and friction sensitivities of BTF-based composite explosives, indicating enhanced safety.

Acknowledgement

This project was supported by the National Natural Science Foundation of China (No.22173086) and Science and Technology Department Project in Sichuan (No.2022NSFSC2015).

References

- [1] Yang, Z.-w.; Wang, Y.-p.; Zhou, J.-h.; Li, H.; Huang, H.; Nie, F. Preparation and Performance of a BTF/DNB Cocystal Explosive. *Propellants Explos. Pyrotech.* **2014**, *39*(1): 9-13; <https://doi.org/10.1002/prop.201300086>.
- [2] Yang, Z.-w.; Li, H.-z.; Zhou, X.-q.; Zhang, C.; Huang, H.; Li, J.; Nie, F. Characterization and Properties of a Novel Energetic-Energetic Cocystal Explosive Composed of HNIW and BTF. *Cryst. Growth Des.* **2012**, *12*(11): 5155-5158; <https://doi.org/10.1021/cg300955q>.
- [3] Dolgoborodov, A.; Brazhnikov, M.; Makhov, M.; Gubin, S.; Maklashova, I. Detonation Performance of High-dense BTF Charges. *J. Phys.: Conf. Ser.* **2014**,

- 500(5): paper 052010; <https://doi.org/10.1088/1742-6596/500/5/052010>.
- [4] Zeng, G.-a.; Nie, F.-d.; Liu, Y. Preparation of ultra-Fine BTF Particles. (in Chinese) *Chin. J. Explos. Propellants (Huozhayao Xuebao)* **2002**, 25(3): 20-22; https://en.cnki.com.cn/Article_en/CJFDTOTAL-BGXB200203007.htm.
- [5] Yue, X.-x.; Luo, Q.-p.; Cui, P.-t.; Li, Z.-q.; Duan, X.-h.; Yin, T. Preparation and Properties of FOX-7 Nanoparticles by Recrystallization at Low Temperature. (in Chinese) *Chin. J. Explos. Propellants (Huozhayao Xuebao)* **2021**, 44(2): 147-153; <http://kns.cnki.net/kcms/detail/detail.aspx?doi=10.14077/j.issn.1007-7812.202009014>.
- [6] Spitzer, D.; Pichot, V.; Berthe, J.-E.; Pessina, F.; Deckert-Gauding, T.; Deckert, V.; Lobry, E.; Comet, M. Nanocrystallization of Energetic Materials by Spray Flash Evaporation for Explosives and Propellants. *Int. J. Energ. Mater. Chem. Propul.* **2019**, 18(4): 325-339; <https://doi.org/10.1615/IntJEnergeticMaterialsChemProp.2019027410>.
- [7] Wang, Z.-q.; Huang, Y.-s.; Li, R.; Mao, L. Preparation and Properties of Al/Bi₂O₃-HNIW Hybrid Composites. (in Chinese) *J. Energ. Mater.* **2020**, 28(12): 1132-1139; <https://doi.org/10.11943/CJEM2020105>.
- [8] Zhu, Y.; Lu, Y.; Gao, B.; Wang, D.; Guo, C.; Yang, G. Synthesis, Characterization, and Sensitivity of a CL-20/PNCB Spherical Composite for Security. *Materials* **2018**, 11(7): 1130; <https://doi.org/10.3390/ma11071130>.
- [9] Wang, J.-y.; Gao, K.; Xu, W.-z.; Ye, B.-y.; Xu, Y. Effect of Calcium Stearate on the Characteristics of CL-20/Estane Composite Particles. (in Chinese) *Chin. J. Explos. Propellants (Huozhayao Xuebao)* **2015**, 4: 22-26; <https://doi.org/10.14077/j.issn.1007-7812.2015.04.005>.
- [10] Ji, W.; Li, X.-d.; Wang, J.-y. Effect of the Spray Drying Technological Conditions on the Particle Size of HMX/F₂₆₀₂ Core-Shell Composite Microspheres. (in Chinese) *J. Energ. Mater.* **2016**, 24(3): 295-299; <https://doi.org/10.11943/j.issn.1006-9941.2016.03.015>.
- [11] Ji, W.; Xu, Y.-x.; Wang, T.; Wang, D.-j. Preparation and Characterization of nano-BTF Explosive by Electrostatic Spray. (in Chinese) *Chin. J. Explos. Propellants (Huozhayao Xuebao)* **2021**, 44(6): 851-855; <https://doi.org/10.14077/j.issn.1007-7812.202103017>.
- [12] Chen, K.; Yuan, S.; Wen, X.-M.; Sang, C.; Luo, Y. Effect of Mixed Isocyanate Curing Agents on the Performance of *In Situ*-Prepared HTPE Binder Applied in Propellant. *Propellants Explos. Pyrotech.* **2021**, 46(3): 428-439; <https://doi.org/10.1002/prop.202000190>.
- [13] Kim, D.W.; Kim, H.; Huh, E.; Park, S.; Lee, C.H.; Ahn, I.S.; Koo, K.K.; Lee, K.D. Estane-assisted Preparation of Submicron β -Form HMX Particles through Antisolvent Crystallization. *Propellants Explos. Pyrotech.* **2021**, 46(6): 944-949; <https://doi.org/10.1002/prop.202000300>.
- [14] Sanyal, B.; Chakravarthy, S.R.; Ramesh, M.V.L.; Agnihorti, G.; Verma, D.K. Tailoring of Mechanical Properties of Highly Filled nano-Aluminized Propellants by Modifying Binder Polymer Microstructure. *Propellants Explos. Pyrotech.* **2020**,

- 45(12): 1959-1971; <https://doi.org/10.1002/prop.202000182>.
- [15] Herman, M.J.; Woznick, C.S.; Scott, S.J.; Tisdale, J.T.; Yeager, J.D.; Duque, A.L. Composite Binder, Processing, and Particle Size Effects on Mechanical Properties of non-Hazardous High Explosive Surrogates. *Powder Technol.* **2021**, *391*: 442-449; <https://doi.org/10.1016/j.powtec.2021.06.009>.
- [16] Zeman, S.; Hussein, A.K.; Jungova, M.; Elbeih, A. Effect of Energy Content of the Nitraminic Plastic Bonded Explosives on Their Performance and Sensitivity Characteristics. *Def. Technol.* **2019**, *15*(4): 488-494; <https://doi.org/10.1016/J.dt.2018.12.003>.

Received: October 17, 2022

Revised: December 8, 2023

First published online: December 21, 2023